Journal of Electrochemistry

Volume 26 | Issue 3

2020-06-28

Ordered Mesoporous Carbon/Graphene/Nickel Foam for Flexible Dopamine Detection with Ultrahigh Sensitivity and Selectivity

Lai-yu WANG

Xin XI

Dong-qing WU

Xiong-yu LIU

Wei JI

Rui-li LIU
2. Laboratory of Aerospace Catalysts and New Materials, Dalian Institute of Chemical Physics, Chinese Academy of Science, Dalian 116023, China;, ruililiu@sjtu.edu.cn

DOI: 10.13208/j.electrochem.190428 **Article ID**:1006-3471(2020)03-0347-12
Cite this: *J. Electrochem*. **2020**, *26*(3): 347-358 **Http**://electrochem.xmu.edu.cn

Ordered Mesoporous Carbon/Graphene/Nickel Foam for Flexible Dopamine Detection with Ultrahigh Sensitivity and Selectivity

WANG Lai-yu[1], XI Xin[1], WU Dong-qing[2], LIU Xiong-yu[1], JI Wei[1], LIU Rui-li[1*]
(1. *Department of Electronic Engineering, Shanghai Jiao Tong University, Shanghai*, 200240, *P. R. China*;
2. *School of Chemistry and Chemical Engineering, Shanghai Jiao Tong University, Shanghai*, 200240, *P. R. China*)

Abstract: Flexible biosensors have received intensive attentions for their potential applications in wearable electronics. To obtain flexible electrochemical dopamine (DA) sensors, the ordered mesoporous carbon/graphene/nickel foam (OMC/G/Ni) composite was fabricated in this work via the growth of graphene on Ni foam by chemical vapor deposition, and the formation of the OMC layer followed by the carbonization of co-assembled resol and block polymer., The monolithic Ni foam in the resultant OMC/G/Ni electrode provided an interconnected metal framework with high conductivity and good flexibility, while the OMC layer with the vertically aligned mesopore arrays rendered the composite a large electroactive surface with highly exposed active sites. More importantly, the graphene sandwiched between the OMC layer and Ni foam greatly enhanced the compatibility of each component. As the integrated electrode in DA sensor, the OMC/G/Ni electrode exhibited excellent performances with a large linear detection range (0.05 ~ 58.75 $\mu mol \cdot L^{-1}$), an ultra-low detection limit (0.019 $\mu mol \cdot L^{-1}$), high selectivity, good reproducibility and high stability, outperforming the recently reported flexible DA sensors. Moreover, the OMC/G/Ni electrode still kept the good DA sensing behavior at its bent states, demonstrating its potential for flexible biosensors.

Key words: ordered mesoporous carbon; graphene; nickel foam; dopamine sensor; flexible electrochemical sensor
CLC Number: O646 **Document Code:** A

Dopamine (DA) is regarded as one of the most important neurotransmitters in human nervous system, mainly due to its vital role in many brain activities and functions[1-4]. Some serious nervous system diseases including depression, Parkinson and Alzheimer are closely related to the abnormal levels of DA activity[5]. Therefore, simple and accurate detection of DA has a high clinical significance. In this respect, diversified DA detection methods such as electrochemical sensing[6-7], fluorescence[8-9], chromatography coupled spectroscopy[10] and surface enhanced Raman scattering[11] have been developed over the last decades. Compared with the spectroscopy based DA sensing strategies, the electrochemical approaches, which are mainly based upon the oxidation-reduction process of DA over the working electrodes, have received more attentions because of their obvious advantages in cost and sensitivity[12-13].

Very recently, accompanying with the intriguing concepts of real-time monitoring and diagnosis, the ever-growing interests in wearable electronics and artificial skins have aroused a high demand on flexible sensors for biological analytes such as DA, ascorbic acid (AA) and uric acid (UA)[14-15]. For this purpose, electrochemical DA sensors are regarded as the appealing candidates because their detection behaviors are mainly determined by the working electrodes and the structural simplicity offers the opportunity to manufacture flexible or miniaturized DA sensors[16-17]. The key to obtain flexible electrochemical DA sensor is the fabrication of bendable working electrodes being able to reserve the sensitivity during the deformation of the sensor.

In this work, we report a step-wise strategy to

Received: 2019-04-28, Revised: 2019-08-02 *Corresponding author, Tel: (86-21)34207045, E-mail: ruililiu@sjtu.edu.cn

fabricate the ordered mesoporous carbon/graphene/nickel foam (OMC/G/Ni) as the electrode for the electrochemical DA sensors. In the integrated OMC/G/Ni electrode, monolithic Ni foam serves as the highly conductive and flexible substrate with three-dimensional (3D) interconnected metal framework. Containing the vertically aligned mesopore arrays with the size of ~ 10 nm, the OMC layer over the whole electrode provides a large electroactive surface with highly exposed active sites for the electrochemical detection of DA. More importantly, the graphene layer sandwiched between the OMC layer and Ni foam can effectively increase the compatibility of each component and enhance sensing ability of the electrode. As the result, the electrochemical sensors with the OMC/G/Ni electrode manifest high sensitivity and selectivity towards DA with a large linear detection range of (0.05 ~ 58.75 μmol·L^{-1}) and a very low detection limit of 0.019 μmol·L^{-1}, outperforming the recently reported flexible DA sensors. Moreover, the OMC/G/Ni electrode can reserve the good DA detection ability even under different bent states, demonstrating its potential for flexible biosensors.

1 Experimental

1.1 Materials and Reagents

Dopamine (DA), ascorbic acid (AA), uric acid (UA), glucose, and triblock copolymer F127 were purchased from Sigma-Aldrich Co., Ltd. Phenol, formaldehyde, sodium chloride (NaCl), sodium hydroxide (NaOH), hydrochloric acid (HCl), disodium hydrogen phosphate (Na_2HPO_4) and sodium dihydrogen phosphate (NaH_2PO_4) were purchased from Sinopharm Chemicals Reagent Co., Ltd. All the reagents were of analytical grade and used as received without further purification. Phosphate buff ered saline solution (PBS, pH = 7.4, 0.1 mol·L^{-1}) was prepared by mixing the stock solutions of Na_2HPO_4 and NaH_2PO_4. The nickel foam (99.8%) was bought from Hefei Kejing Materials Technology Co., Ltd. Deionized water was used throughout the experiments.

1.2 Apparatus

Field emission-scanning electron microscopic (FE-SEM) images were obtained on a JSM-7401F (JEOL Ltd., Japan) microscope at a voltage of 3 kV. Raman spectra were recorded on a Senterra R200-L (Bruker Optics, Germany) with the excitation from 532 nm line of an Ar-ion laser (5 mW). X-ray diffraction (XRD) patterns were recorded on a Bruker D8 Advance powder Diffractometer (Bruker, Germany) using Cu K_α radiation (40 kV, 35 mA) at the scan rate of 5° min^{-1} from 10° to 80° (2θ). Transmission electron microscopic (TEM) measurements were conducted on a JEM-2010F (JEOL, Japan) operated at an accelerating voltage of 200 kV. Before the TEM measurements, OMC/G/Ni was etched with HCl solution (3 mol·L^{-1}) at 80 oC for 5 h to remove the Ni component. The resulting sample was suspended in ethanol and then transferred onto a Cu grid for TEM characterizations. The X-ray photoelectron spectra (XPS) were collected on ESCALAB 250Xi instrument (Thermo Fisher Scientific, USA) with a monochromatic Al K_α X-ray source. Nitrogen absorption isotherms were measured on an ASAP 2460 (Micromeritics Instrument Corp, USA). The samples were degassed in a vacuum at 200 °C for about 12 h before measurements.

Cyclic voltammetry (CV), differential pulse voltammetry (DPV), electrochemical impedance spectroscopy (EIS) and amperometry tests were carried out with a CHI 760E electrochemical workstation (Shanghai Chenhua Limited Co.) under ambient conditions. In a three-electrode system, a piece of OMC/G/Ni served as the working electrode, while a platinum wire and a Ag/AgCl electrode (3 mol·L^{-1} KCl) as the counter electrode and the reference electrode, respectively. All the measurements were performed in a stirred PBS (pH = 7.4, 0.1 mol·L^{-1}) solution.

1.3 Syntheses of Ordered Mesoporous Carbon/Graphene/Nickel Foam (OMC/G/Ni)

The composites of graphene and nickel foam (G/Ni) were fabricated by a typical chemical vapor deposition (CVD) method[18]. Firstly, a piece of nickel foam (4 cm × 3 cm × 1 mm) was squashed to ~ 0.1 mm by a hot pressing process at 15 MPa, and then heated to 1000 ℃ in a tubular furnace under the flows of H_2 (20 sccm) and Ar (180 sccm). After an-

nealing at 1000 ℃ for 10 min, methane (15 sccm) was introduced into the tubular furnace as the carbon source for 10 min for the growth of graphene. After rapidly cooled down to room temperature, graphene wrapped nickel foam (G/Ni) could be obtained as a piece of black monolith.

Typically, phenol (3 g), formaldehyde (37wt.% in water, 10.5 mL) and the aqueous solution of NaOH (0.1 mol·L^{-1}, 75 mL) were firstly mixed in a round-bottom flask, and the mixture was heated to 70 ℃ for about 30 min to produce low-molecular-weight phenolic resols. Consequently, the phenolic resol solution (18 g) was mixed with the aqueous solution of F127 (6wt.%, 15 mL). The resulting mixture was diluted with deionized water (50 mL), and the mixed solution was then stirred at 67 ~ 70 ℃ for 10 ~ 14 h until the color turned to crimson, indicating the formation of resol-F127 monomicelles[19].

The as-prepared solution of resol-F127 monomicelles (7 mL) was diluted with deionized water (23 mL) and then transferred into a Teflon lined stainless steel autoclave. Subsequently, a piece of G/Ni (1 cm × 1.5 cm) was immersed in the solution for 3 h to allow sufficient contact between each component. Consequently, the mixture was hydrothermally treated for 20 h at 130 ℃. After being cooled to room temperature, the resulting sample was washed by water, dried in a vacuum oven and calcinated at 750 ℃ for 2 h (heating rate = 5 ℃·min^{-1}) under Ar atmosphere to produce the OMC/G/Ni composite with the sizes of 1 cm × 1.5 cm × 0.1 mm.

2 Results and Discussion

2.1 Characterizations

The conductivity, structure and surface morphology of the working electrodes in the electrochemical DA sensors are the major factors influencing the detection performances of the sensors[20]. Ordered mesoporous carbons (OMCs) possess many intriguing features including uniform porous structure, highly electro-active surface area, enhanced electron transfer ability and high chemical stability, which make them attractive electrode materials for the electrochemical DA sensor[21-23]. Nevertheless, most OMC materials are in the form of powders and flakes, and their utilization in flexible electrodes needs the assistance of binders, which will inevitably reduce the sensing activity of the resulting sensors[24-27]. To avoid the unnecessary additives in the electrodes, an interface-induced self-assembly approach is adopted in this work to directly grow OMC on the substrate surface, which can ensure the formation of the integrated electrodes with OMC decorated surfaces. In this respect, nickel (Ni) foam is selected as the substrate. The highly interconnected metal framework of Ni foam has both high conductivity and macroporous scaffold. The coating of an OMC layer over it will generate a hierarchically porous structure for the resulting electrode, which can effectively facilitate the transportation of charge carriers and analyte molecules. Between the Ni foam and OMC, graphene is introduced by chemical vapor deposition (CVD) method, which is expected to enhance the interactions between the different components in the electrode and improve the performances of the electrode.

According to the aforementioned electrode design, the fabrication processes of the flexible OMC/G/Ni electrodes are illustrated in Fig. 1. Firstly, graphene was grown on the surface of Ni foam via the classic CVD approach to produce the graphene wrapped Ni foam (G/Ni). Consequently, G/Ni was immersed in the solution containing the monomicelles of triblock copolymer F127 and low-molecular-weight phenolic resols. The mixture was hydrothermally treated at 130 ℃ to allow the deposition of the resol/F127 monomicelles on the surface of G/Ni and the further solidification of the resols[19]. After that, the composite of the monomicelles and G/Ni were thermally treated at 750 ℃ under an inert atmosphere. During this process, the carbonization of resol and decomposition of F127 led to the formation of an OMC layer over the surface of the G/Ni substrates, which, thus, generate OMC/G/Ni as the product. To specify the role of graphene in the OMC/G/Ni composite, a reference sample with the OMC layer directly grown on the surface of Ni foam was fabricated in the controlled experiments (Supporting Information),

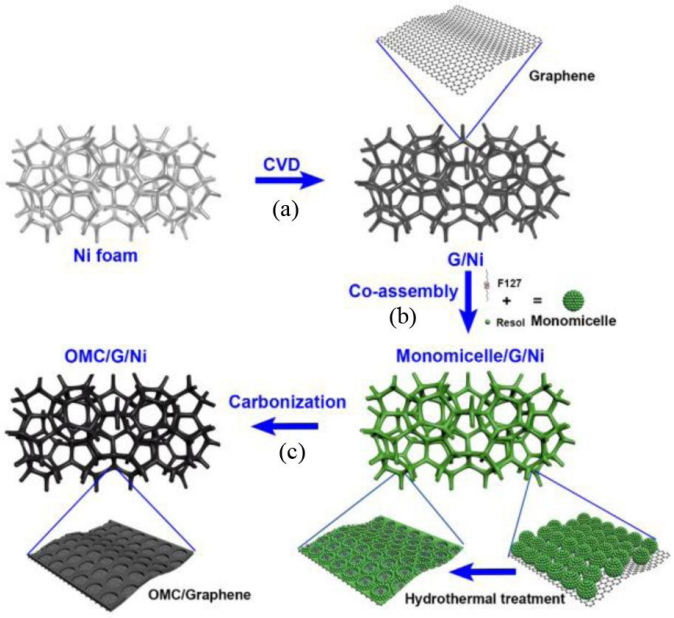

Fig. 1 The schematic illustration of the fabrication processes for the flexible OMC/G/Ni electrode. a) the CVD process for the preparation of graphene wrapped Ni foam (G/Ni); b) the deposition of resol-F127 monomicelles on the surface of G/Ni; c) the carbonization of the monomicelle/G/Ni composite to produce OMC/G/Ni.

which is accordingly named as OMC/Ni.

The microstructures and morphologies of G/Ni, OMC/Ni and OMC/G/Ni were first characterized by field emission scanning electron microcopy (FE-SEM) and transmission electron microscopy (TEM). As illustrated in the SEM images of G/Ni (Fig.s S1A and S1B in the Supporting Information), graphene sheets with a few wrinkles were uniformly wrapped around the surface of Ni foam, confirming the successful CVD growth of graphene. The visible ripples and wrinkles in graphene were caused by different thermal expansion of Ni foam and graphene, which is a typical feature of the CVD-derived graphene[28-29]. After the hydrothermal treatment, the OMC/G/Ni electrode still reserved the macroporous structure of the Ni foam (Fig. 2A). Moreover, the SEM images with higher magnifications (Fig.s 2B, 2C and S2) indicate that the surface of the G/Ni foam was covered with a layer of porous carbon. A closer observation of the carbon layer (Fig. 2D) reveals that it had vertically aligned mesopores with the diameter of ~10 nm, which were arranged in a highly ordered hexagonal pattern.

The N_2 adsorption and desorption measurements of the OMC/G/Ni display a type-II isotherm with H_2 hysteresis loop (Fig. S3), which is similar to the recently reported thin-layer mesoporous materials[30-32]. To clarify the mesoporous structure, a piece of OMC/G/Ni was further treated by hydrochloric acid at 80 oC for 5 h to remove the Ni substrate. The remaining contents with graphene and OMC were then transferred to a copper grid for TEM characterization. In accordance with the SEM results, the TEM images (Fig.s 2E and 2F) also show the existence of the perpendicularly aligned mesopore arrays in the residue sheets from the acid-etched OMC/G/Ni. In contrast, the surface morphology of OMC/Ni differed from that of OMC/G/Ni. Although vertical mesopores could also be found on the surface of OMC/Ni (Fig.s S1C and S1D), many disordered broken parts with the sizes of ~ 100 nm were observed in the OMC layer. It should be noted that the OMC in OMC/Ni was directly grown on the surface of Ni foam without the assistance of graphene. Therefore, the different surface morphologies of OMC/G/Ni and OMC/Ni could be attributed to the graphene content. As indicated in our previous work, the assembly behavior of the resol/F127 monomicelles depended on the properties of the substrates[30-31]. Without the graphene layer, the

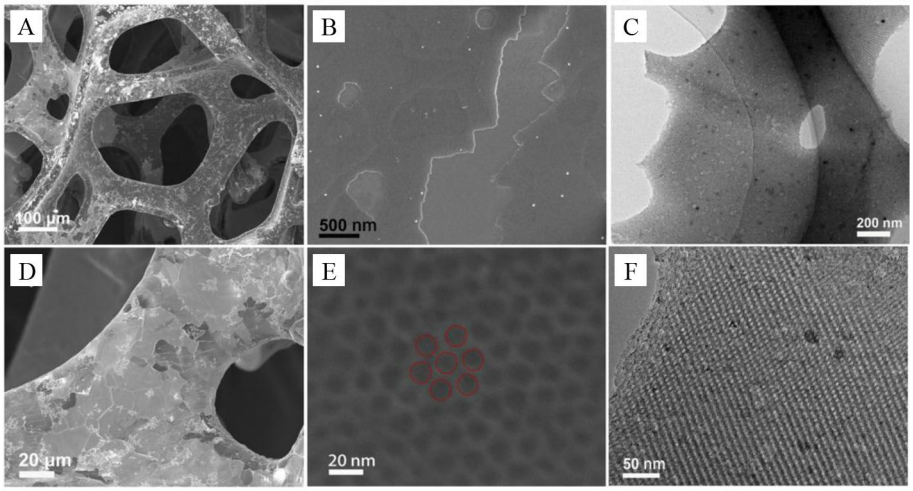

Fig. 2 Morphology and structure characterization of OMC/G/Ni. A-D) SEM images of OMC/G/Ni with different magnifications. E) and F) TEM images of OMC/G composites (after the etching of Ni foam) with different magnifications.

Ni foam alone was not favourable for the homogenous deposition of the monomicelles, leading to the formations of voids and defects in the OMC layer. In contrast, a graphene layer could absorb the resol/F127 monomicelles via noncovalent forces such as π-π interactions and hydrophobic interactions, which can, therefore, improve the compatibility between each component and result in the uniform packing of the monomicelles over the surface of G/Ni.

Raman spectroscopy and X-ray diffraction (XRD) were subsequently applied to survey the microstructures of the samples. In the Raman spectra of OMC/Ni (Fig. S4A), the two peaks at ~ 1350 and ~ 1590 cm^{-1} could be assigned to the characteristic D band and G band of carbon, respectively, which are similar to the previously reported mesoporous carbon[31-32]. Differently, only G and 2D bands could be observed in the Raman spectra of G/Ni, which suggests the high quality of the graphene layer[33]. Furthermore, the integrated intensity ratio of the G and 2D bands (I_G/I_{2D}) is ~ 2.69, suggesting the existence of a multi-layer graphene in G/Ni[28,34]. Compared with the Raman profile of G/Ni, a pronounced D band at ~ 1350 cm^{-1} can be observed in the Raman spectra of OMC/G/Ni, which can be attributed to the introduction of OMC layer. On the other hand, the XRD patterns of G/Ni, OMC/Ni and OMC/G/Ni (Fig. S4B) are all dominated by three strong peaks at $2\theta \approx 44°$, 51° and 76°, which belong to the diffractions from the Ni substrates[35]. In addition, the weak diffraction peaks around 26.5° can be found in the XRD profiles of OMC/Ni and OMC/G/Ni (Fig. S4C), which should be the typical (002) planes of their OMC layers[30].

2.2 Electrochemical Performances

The electrochemical DA sensing behaviors of the obtained electrodes were firstly measured by recording their cyclic voltammetric (CV) profiles in phosphate-buffered saline (PBS, pH = 7.4, 0.1 mol·L^{-1}) in the presence of DA (100 μmol·L^{-1}) at a scan rate of 50 mV·s^{-1} (Fig. 3A). In the CV curve of OMC/G/Ni, a distinct oxidation peak can be observed at 0.20 V, and the corresponding reduction peak is located at 0.15 V, which are attributable to the oxidation/reduction processes of DA on the surface of OMC/G/Ni (Scheme S1). In contrast, the CV profile of OMC/Ni only has a very weak redox couple of DA at the corresponding potentials, suggesting a much weaker electrochemical DA sensing ability than OMC/G/Ni. In the absence of the OMC content, G/Ni only delivers a structure-less CV curve without obvious oxidation or reduction peaks, implying the absence of electrochemical responses towards DA. The poor electrochemical sensitivity of the G/Ni electrode should be due to the lack of defects such as oxygen containing groups in the graphene layer, which is crucial for the catalytic activity of the carbonaceous electrodes in

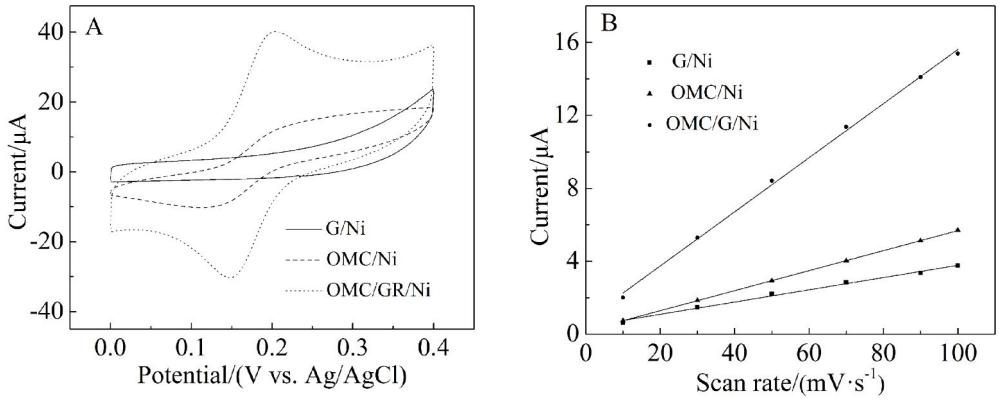

Fig. 3 A) CV curves of G/Ni, OMC/Ni and OMC/G/Ni in PBS (pH = 7.4, 0.1 mol·L^{-1}) containing DA (100 μmol·L^{-1}) at a scan rate of 50 mV·s^{-1}. B) The plots of capacitive current (I_{anodic}-$I_{cathodic}$) versus scan rate.

electrochemical sensing systems[15].

The different DA sensing activities of the three electrodes can be explained by their electrochemical active surface areas (ECSAs). Deduced from the results in Fig. 3B (Supporting Information)[36-37], the ECSA of OMC/G/Ni is ~ 7.432 cm^2·g^{-1}, much higher than those of OMC/Ni (2.774 cm^2·g^{-1}) and G/Ni (1.677 cm^2·g^{-1}), which can render the efficient contact between active sites and analyte molecules. The differences among the three electrodes are also manifested in their electrochemical impedance spectra (EIS). Generally, a semicircle in Nyquist plot can be attributed to the charge-transfer resistance (R_{ct}) within the electrode. As shown in Fig. S5, the R_{ct} of OMC/G/Ni is 1.8 Ω, much less than those of G/Ni (309.2 Ω) and OMC/Ni (6.5 Ω), which indicates the presence of OMC and graphene could effectively reduce the Rct of the electrode[38-39] and accelerate the charge transfer kinetics[40]. Moreover, the low frequency part of the oblique curves from OMC/G/Ni and OMC/Ni shows a higher slope than G/Ni, revealing the decreased obstruction for ionic movement. Therefore, the excellent DA sensing activities of OMC/G/Ni can be assigned to the synergetic effects of its structures and compositions. Firstly, the introduction of the OMC layer can efficiently increase the surface area of the electrode and enhance the exposure of the active sites. On the other hand, the graphene between the OMC layer and the Ni foam can improve the compatibility between each component and increase the conductivity of the whole electrode.

Encouraged by the highest DA sensing ability of OMC/G/Ni among the obtained electrodes, its electrochemical responses towards DA at different scan rates in the range of 20 ~ 200 mV·s^{-1} were further recorded. As shown in Fig. 4A, the intensities in both anodic and catholic peak currents of OMC/G/Ni show the obvious upward trends with the increased scan rate. More importantly, the calibration plots of the redox peak currents (I_{pa} & I_{pc}) manifest linear correlations with the scan rates (Fig. 4B). Accordingly, the calibration equations are calculated as I_{pa} = 6.114+ 0.155v (R^2 = 0.996) and I_{pc}= -4.351-0.167v (R^2 = 0.995), indicating that the electrochemical DA detection behavior of OMC/G/Ni is an adsorption-controlled process[41].

Consequently, differential pulse voltammetric (DPV) profiles of OMC/G/Ni were measured to further examine its electrochemical detection activity towards DA. As found in Fig.s 5A and 5B, the current densities of the DA oxidation peaks gradually increased with the variation of the DA concentration. The increased trend in the current density can still be observed with the DA concentration in a very low range from 0.05 to 1 μmol·L^{-1}. The current density and the DA concentration can be linearly fitted, as seen in Fig. 5C, with the equation of I_p = 2.40 + 0.89 CDA (R^2 = 0.996). The excellent DA sensing ability of OMC/G/Ni can also be confirmed by recording its amperometric responses on the successive injections

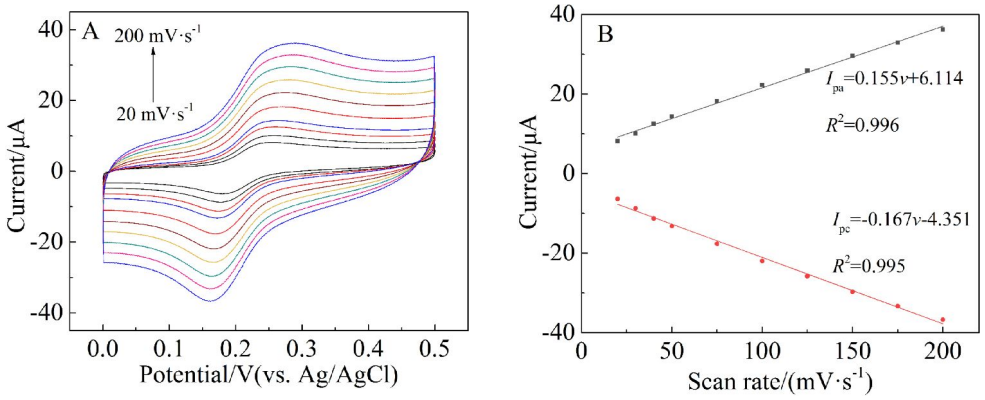

Fig. 4 A) CV curves of the OMC/G/Ni electrode in PBS (0.1 mol·L^{-1}, pH = 7.4) with DA (50 μmol·L^{-1}) at different scan rates: 20, 30, 40, 50, 75, 100, 125, 150, 175 and 200 mV·s^{-1}. B) The fitting lines for the anodic and catholic peak currents versus scan rate.

of DA in a homogeneously stirred PBS solution. At the potential of + 0.2 V, OMC/G/Ni can deliver an instant response current when the concentrations of DA in PBS are varying from 0.05 to 10 μmol·L^{-1} (Fig. 5D). Even when the DA concentration is as low as 0.05 μmol·L^{-1}, an amperometric response can still be observed (the inset of Fig. 5D), indicating the high sensitivity of the OMC/G/Ni electrode. The calibration plot of *i*-*t* current versus DA concentration also follows a linear relationship (Fig. 5E) and the corresponding regression equation can be expressed by $I_p = 9.50 + 1.04C_{DA}$ ($R^2 = 0.996$). As the result, the linear detection of OMC/G/Ni towards DA ranges from 0.05 to 58.75 μmol·L^{-1} with the detection limit as low as 0.019 μmol·L^{-1} and the signal-to-noise (*S*/*N*) ratio of 3.

Since other chemicals such as glucose, uric acid (UA), sodium chloride (NaCl) and ascorbic acid (AA) often coexist with DA in body fluids, the selectivity of the DA sensors is also an important parameter for their performances. Therefore, the amperometric responses of OMC/G/Ni was further measured in the presence of common interfering analyte molecules in PBS solution (pH = 7.4, 0.1 mol·L^{-1}) to clarify its selectivity towards DA. As indicated in Fig. 5F, the OMC/G/Ni electrode shows a remarkable amperometric response immediately with the addition of DA. However, the injections of other chemicals in the sequence of glucose, UA, NaCl and AA barely cause any current changes in the *i*-*t* curve until another portion of DA is added to the PBS solution, suggesting the good selectivity of the OMC/G/Ni electrode.

The excellent selectivity of the OMC/G/Ni electrode towards DA can be attributed to the abundant oxygen-containing groups (C-O, C=O, and O=C-O, Fig. S6) in the resol-derived OMC layer and the low operation voltage (+0.2 V) during the sensing process[42-44]. As the disrupting analytes in the sensing system, UA and AA are negatively charged molecules, while DA is a neutral one. Therefore, the oxygen-containing groups in the surface of the OMC/G/Ni electrode will block the access of UA or AA due to the repulsion between them and these analytes, which could be effectively improve the selectivity of the electrode[42-43]. On the other hand, the operation voltage (+0.2 V) of the three-electrode sensing system is much lower than the oxidation voltage of glucose, causing no current response at the electrode during the sensing process[44].

Besides the sensitivity and selectivity, the reproducibility and stability are also vital for electrochemical DA sensors. In this respect, the CV curves of the five independent OMC/G/Ni electrodes were measured in PBS solution with DA (50 μmol·L^{-1}). As shown in Fig. S7, the five electrodes deliver very similar CV curves, suggesting the good reproducibility of the OMC/G/Ni electrodes. According to the corre-

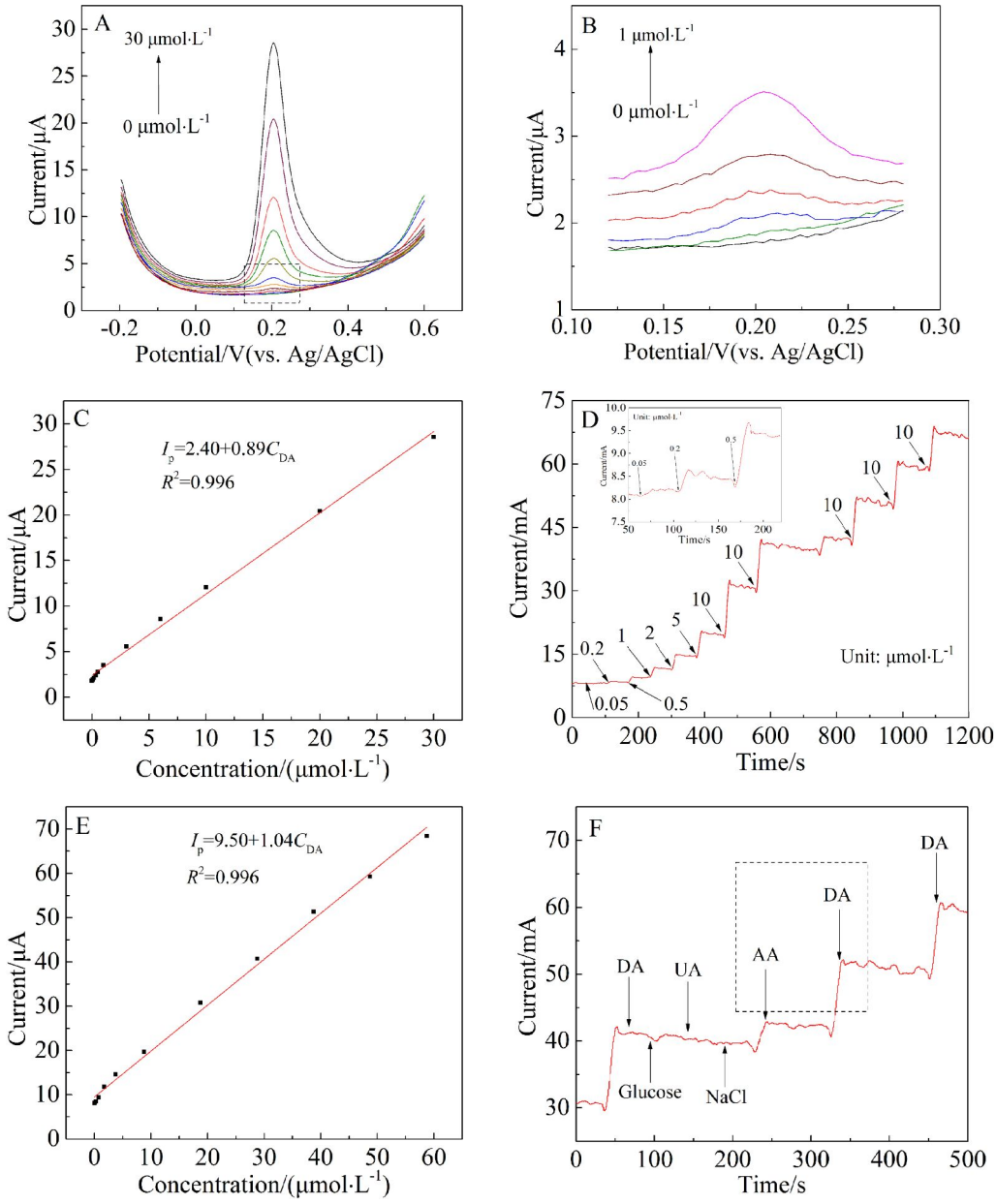

Fig. 5 A) DPV curves of OMC/G/Ni in PBS (0.1 mol·L^{-1}, pH = 7.4) solution with the DA concentrations in the range of 0 ~ 30 μmol·L^{-1}. B) Magnified DPV curves with the DA concentrations of 0, 0.05, 0.15, 0.3, 0.5, and 1.0 μmol·L^{-1}. C) Calibration plot of the peak current to DA concentration. D) The amperometric (*i-t*) curve of OMC/G/Ni upon addition of DA at 0.2 V. Inset: Magnified *i-t* curve upon the addition of DA at 0.05, 0.2 and 0.5 μmol·L^{-1}. E) Calibration plot of *i-t* current to the DA concentration. F) Amperometric responses of OMC/G/Ni with the successive injections of DA, Glucose, UA, NaCl, AA, DA and DA (All the concentrations of the added analytes are 10 μmol·L^{-1} in the resulting PBS).

sponding oxidation peak currents, the relative standard deviation (RSD) of OMC/G/Ni is only ~ 2.0%. On the other hand, the operation stability of OMC/G/Ni was studied by the continuous CV scans at a scan rate of 50 mV·s^{-1} for 100 cycles in PBS solution with DA (50 μmol·L^{-1}). The oxidation peak current of OMC/G/Ni still keeps ~ 87% of initial intensity after 100 CV scans (Fig. 6A). Additionally, the long term storage stability of the OMC/G/Ni electrode is evaluated by comparing the current density of its oxidation peak towards DA every other day. And no obvious change could be found after 17 d (Fig. 6B), suggesting

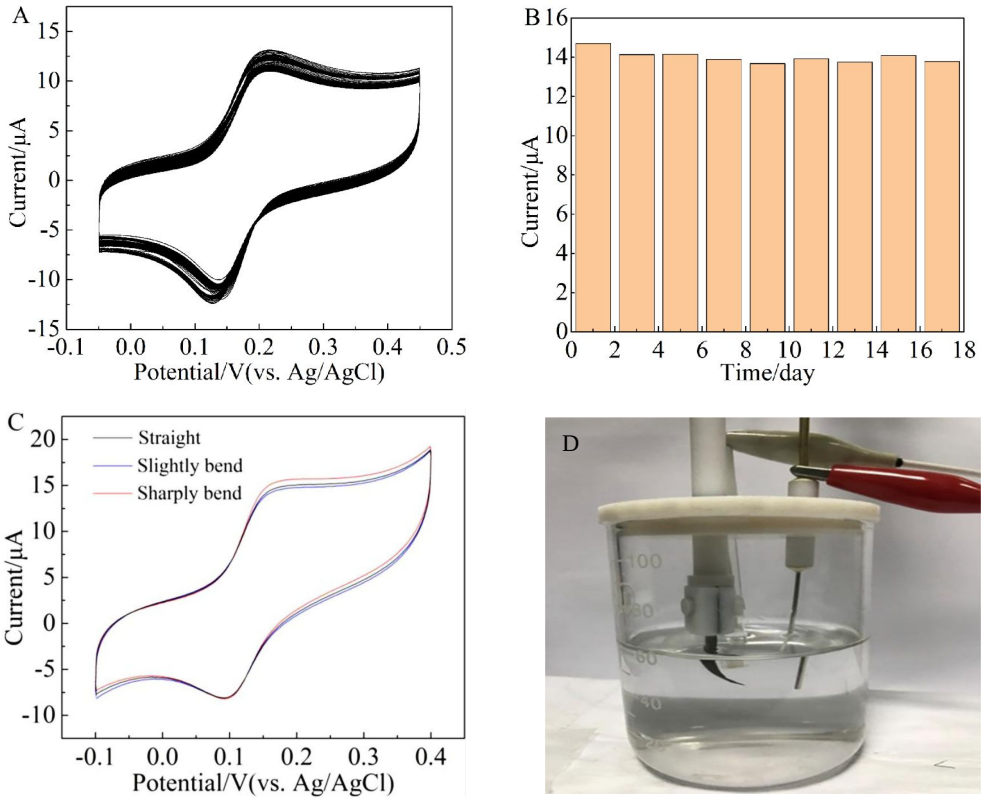

Fig. 6 Stability tests of the OMC/G/Ni electrode. A) CV profiles for 100 scanning cycles at a scan rate of 50 mV·s^{-1}; B) Current responses every other day in PBS (0.1 mol·L^{-1}, pH = 7.4) with DA (50 μmol·L^{-1}). C) CV curves under different bent states; D) Photograph showing the slightly bent electrode.

its good storage stability[45-46].

The ability to work under bent states is very essential for flexible electrochemical sensors[47]. Therefore, the CV profiles of OMC/G/Ni at different bent states were recorded in PBS solution (0.1 mol·L^{-1}) with DA (50 μmol·L^{-1}). As displayed in Fig.s 6C, 6D and S8, the redox peaks are barely changed at the three bent states, confirming the excellent flexibility of the OMC/G/Ni electrode. As summarized in Tab. S1, the excellent sensing performances of OMC/G/Ni outperform the recently reported flexible DA sensors in terms of detection limit and selectivity.

The detection ability of OMC/G/Ni towards DA in a real sample were evaluated by using standard addition method[48]. As summarized in Tab. S2, the sensor with OMC/G/Ni electrode shows excellent DA sensing performances with the appropriate recovery of 97.6% ~ 103.2% and the RSD below 3.6%, confirming the reliability and effectiveness of the OMC/G/Ni based sensor for the practical detection of DA.

3 Conclusions

In this work, the OMC/G/Ni composite was manufactured by the first CVD growth on a graphene layer over Ni foam, and followed by the subsequent formation of an OMC layer via a co-assembly route. As the flexible electrode for the electrochemical DA detection, the OMC/G/Ni composite manifested excellent performances with a large linear detection range, an ultra-low detection limit, high selectivity, good reproducibility and high stability, which could be attributable to the combination of 3D macroporous framework of Ni foam and highly ordered mesopore arrays of OMC by the mediation of graphene. Moreover, the OMC/G/Ni electrode still exhibited good DA sensing behavior under different bent states, proving its potential application in flexible DA sensors. Based on the unique electrode structure, the further modification of the OMC layer in OMC/G/Ni is

exp ected to bring forwards more high performance electrodes for various flexible electrochemical biosensors.

Acknowledgements

This work was financially supported by National Natural Science Foundation of China (No. 61575121, No. 51772189, No. 21720102002, No. 21772120, No. 21572132), and Shanghai Committee of Science and Technology (No. 16JC1400703).

Supporting Information

Additional experimental data and SEM images. This material is available free of charge via the internet at http://www.electrochem.xmu.edu.cn.

References:

[1] Diaz-Diestra D, Thapa B, Beltran-Huarac J, et al. L-cysteine capped ZnS:Mn quantum dots for room-temperature detection of dopamine with high sensitivity and selectivity [J]. Biosensors & Bioelectronics, 2017, 87: 693-700.

[2] Guan L H(关利浩), Wang C(王超), Zhang W(张望), et al. A facile strategy for two-step fabrication of gold nanoelectrode for in vivo dopamine detection[J]. Journal of Electrochemistry(电化学), 2019, 25(2): 244-251.

[3] Taylor I M, Robbins E M, Catt K A, et al. Enhanced dopamine detection sensitivity by PEDOT/graphene oxide coating on *in vivo* carbon fiber electrodes[J]. Biosensors and Bioelectronics, 2017, 89: 400-410.

[4] Dong P F(董鹏飞), Li N(李娜), Zhao H Y(赵海燕), et al. Synthesis of keggin polyoxometalates modified carbon paste electrode as a sensor for dopamine detection[J]. Journal of Electrochemistry(电化学), 2018, 24(5): 555-562.

[5] Huang S, Song S S, Yue H Y, et al. ZnO nanosheet balls anchored onto graphene foam for electrochemical determination of dopamine in the presence of uric acid[J]. Sensors and Actuators B: Chemical, 2018, 277: 381-387.

[6] Chen P Y, Vittal R, Nien P C, et al. Enhancing dopamine detection using a glassy carbon electrode modified with MWCNTs, quercetin, and Nafion®[J]. Biosensors and Bioelectronics, 2009, 24(12): 3504-3509.

[7] Gao G, Zhang Z K, Wang K, et al. One-pot synthesis of dendritic Pt_3Ni nanoalloys as nonenzymatic electrochemical biosensors with high sensitivity and selectivity for dopamine detection[J]. Nanoscale, 2017, 9(31): 10998-11003.

[8] Chen J L, Yan X P, Meng K, et al. Graphene oxide based photoinduced charge transfer label-free near-infrared fluorescent biosensor for dopamine[J]. Analytical Chemistry, 2011, 83(22): 8787-8793.

[9] Qu K G, Wang J S, Ren J S, et al. Carbon dots prepared by hydrothermal treatment of dopamine as an effective fluorescent sensing platform for the label-free detection of iron (III) ions and dopamine[J]. Chemistry - A European Journal, 2013, 19(22): 7243-7249.

[10] Cheuk M Y, Lo Y C, Poon W T. Determination of urine catecholamines and metanephrines by reversed-phase liquid chromatography-tandem mass spectrometry [J]. Chinese Journal of Chromatograph, 2017, 35(10): 1042-1047.

[11] Tang L J, Li S, Han F, et al. SERS-active Au@Ag nanorod dimers for ultrasensitive dopamine detection[J]. Biosensors and Bioelectronics, 2015, 71: 7-12.

[12] Zan X L, Bai H W, Wang C X, et al. Graphene paper decorated with a 2D array of dendritic platinum nanoparticles for ultrasensitive electrochemical detection of dopamine secreted by live cells[J]. Chemistry - A European Journal, 2016, 22(15): 5204-5210.

[13] Das A K, Kuchi R, Van P C, et al. Development of an Fe_3O_4@Cu silicate based sensing platform for the electrochemical sensing of dopamine[J]. RSC Advances, 2018, 8(54): 31037-31047.

[14] Yang Y R, Gao W. Wearable and flexible electronics for continuous molecular monitoring[J]. Chemical Society Reviews, 2019, 48(6): 1465-1491.

[15] Cai W H, Lai T, Du H J, et al. Electrochemical determination of ascorbic acid, dopamine and uric acid based on an exfoliated graphite paper electrode: A high performance flexible sensor[J]. Sensors and Actuators B: Chemical, 2014, 193: 492-500.

[16] Hsu M S, Chen Y L, Lee C Y, et al. Gold nanostructures on flexible substrates as electrochemical dopamine sensors[J]. ACS Applied Materials & Interfaces, 2012, 4(10): 5570-5575.

[17] Liu J, He Z M, Xue J W, et al. A metal-catalyst free, flexible and free-standing chitosan/vacuum-stripped graphene/polypyrrole three dimensional electrode interface for high performance dopamine sensing[J]. Journal of Materials Chemistry B, 2014, 2(17): 2478-2482.

[18] Chen Z P, Ren W C, Gao L B, et al. Three-dimensional flexible and conductive interconnected graphene networks grown by chemical vapour deposition[J]. Nature Materials, 2011, 10(6): 424-428.

[19] Fang Y, Gu D, Zou Y, et al. a low-concentration hydrothermal synthesis of biocompatible ordered mesoporous carbon nanospheres with tunable and uniform size [J]. Angewandte Chemie International Edition, 2010, 49 (43): 7987-7991.

[20] Sajid M, Nazal M K, Mansha M, et al. Chemically modified electrodes for electrochemical detection of dopamine in the presence of uric acid and ascorbic acid: A review [J]. TrAC Trends in Analytical Chemistry, 2016, 76: 15-29.

[21] Ndamanisha J C, Guo L P. Ordered mesoporous carbon for electrochemical sensing: A review[J]. Analytica Chimica Acta, 2012, 747: 19-28.

[22] Hartmann M. Ordered mesoporous materials for bioadsorption and biocatalysis[J]. Chemistry of Materials, 2005, 17(18): 4577-4593.

[23] Zhou M, Shang L, Li B L, et al. The characteristics of highly ordered mesoporous carbons as electrode material for electrochemical sensing as compared with carbon nanotubes[J]. Electrochemistry Communications, 2008, 10 (6): 859-863.

[24] Yan X, Bo X J, Guo L P. Electrochemical behaviors and determination of isoniazid at ordered mesoporous carbon modified electrode[J]. Sensors and Actuators B: Chemical, 2011, 155(2): 837-842.

[25] Jia N Q, Wang Z Y, Yang G F, et al. Electrochemical properties of ordered mesoporous carbon and its electroanalytical application for selective determination of dopamine [J]. Electrochemistry Communications, 2007, 9(2): 233-238.

[26] Zhou M, Shang L, Li B L, et al. Highly ordered mesoporous carbons as electrode material for the construction of electrochemical dehydrogenase- and oxidase-based biosensors[J]. Biosensors and Bioelectronics, 2008, 24(3): 442-447.

[27] Ya Y, Wang T S, Xie L P, et al. Highly sensitive electrochemical sensor based on pyrrolidinium ionic liquid modified ordered mesoporous carbon paste electrode for determination of carbendazim[J]. Analytical Methods, 2015, 7(4): 1493-1498.

[28] Zhu G Y, He Z, Chen J, et al. Highly conductive three-dimensional MnO_2-carbon nanotube-graphene-Ni hybrid foam as a binder-free supercapacitor electrode[J]. Nanoscale, 2014, 6(2): 1079-1085.

[29] Chae S J, Günes F, Kim K K, et al. Synthesis of large-area graphene layers on poly-nickel substrate by chemical vapor deposition: wrinkle formation[J]. Advanced Materials, 2009, 21(22): 2328-2333.

[30] Liu R L, Wan L, Liu S Q, et al. An interface-induced co-assembly approach towards ordered mesoporous carbon/graphene aerogel for high-performance supercapacitors[J]. Advanced Functional Materials, 2015, 25(4): 526-533.

[31] Xi X, Wu D Q, Han L, et al. Highly uniform carbon sheets with orientation-adjustable ordered mesopores [J]. ACS Nano, 2018, 12(6): 5436-5444.

[32] Fang Y, Lv Y Y, Che R C, et al. Two-dimensional mesoporous carbon nanosheets and their derived graphene nanosheets: synthesis and efficient lithium ion storage[J]. Journal of the American Chemical Society, 2013, 135(4): 1524-1530.

[33] Bai Y, Wang W Q, Wang R R, et al. Controllable synthesis of 3D binary nickel-cobalt hydroxide/graphene/nickel foam as a binder-free electrode for high-performance supercapacitors[J]. Journal of Materials Chemistry A, 2015, 3(23): 12530-12538.

[34] Dong X C, Ma Y W, Zhu G Y, et al. Synthesis of graphene-carbon nanotube hybrid foam and its use as a novel three-dimensional electrode for electrochemical sensing [J]. Journal of Materials Chemistry, 2012, 22(33): 17044-17048.

[35] Yu M, Chen J P, Liu J H, et al. Mesoporous $NiCO_2O_4$ nanoneedles grown on 3D graphene-nickel foam for supercapacitor and methanol electro-oxidation[J]. Electrochimica Acta, 2015, 151: 99-108.

[36] He P, Yu X Y, Lou X W. Carbon-incorporated nickel-cobalt mixed metal phosphide nanoboxes with enhanced electrocatalytic activity for oxygen evolution[J]. Angewandte Chemie International Edition, 2017, 56(14): 3897-3900.

[37] Wang X L, Li Q, Pan H Y, et al. Size-controlled large-diameter and few-walled carbon nanotube catalysts for oxygen reduction[J]. Nanoscale, 2015, 7(47): 20290-20298.

[38] Shen Y, Sheng Q L, Zheng J B. A high-performance electrochemical dopamine sensor based on a platinum-nickel bimetallic decorated poly(dopamine)-functionalized reduced graphene oxide nanocomposite[J]. Analytical Methods, 2017, 9(31): 4566-4573.

[39] Fan H Q, Quan L X, Yuan M Q, et al. Thin Co_3O_4 nanosheet array on 3D porous graphene/nickel foam as a binder-free electrode for high-performance supercapacitors[J]. Electrochimica Acta, 2016, 188: 222-229.

[40] Walcarius A. Recent trends on electrochemical sensors based on ordered mesoporous carbon[J]. Sensors, 2017, 17 (8): 1863.

[41] Zhang X, Zhang Y C, Ma L X. One-pot facile fabrication of graphene-zinc oxide composite and its enhanced sensitivity for simultaneous electrochemical detection of ascorbic acid, dopamine and uric acid[J]. Sensors and Actuators B: Chemical, 2016, 227: 488-496.

[42] Liu X Y, Xi X, Chen C L, et al. Ordered mesoporous carbon-covered carbonized silk fabrics for flexible electrochemical dopamine detection[J]. Journal of Materials Che-

mistry B, 2019, 7(13): 2145-2150.

[43] Jothi L, Neogi S, Jaganathan S K, et al. Simultaneous determination of ascorbic acid, dopamine and uric acid by a novel electrochemical sensor based on N_2/Ar RF plasma assisted graphene nanosheets/graphene nanoribbons[J]. Biosensors and Bioelectronics, 2018, 105, 236-242.

[44] Wang Y, Li Y M, Tang L H, et al. Application of graphene-modified electrode for selective detection of dopamine [J]. Electrochemistry Communications, 2009, 11(4): 889-892.

[45] Numan A, Shahid M M, Omar F S, et al. Facile fabrication of cobalt oxide nanograin-decorated reduced graphene oxide composite as ultrasensitive platform for dopamine detection[J]. Sensors and Actuators B: Chemical, 2017, 238: 1043-1051.

[46] Thanh T D, Balamurugan J, Lee S H, et al. Effective seed-assisted synthesis of gold nanoparticles anchored nitrogen-doped graphene for electrochemical detection of glucose and dopamine[J]. Biosensors and Bioelectronics, 2016, 81: 259-267.

[47] Gao W, Emaminejad S, Nyein H Y Y, et al. Fully integrated wearable sensor arrays for multiplexed *in situ* perspiration analysis[J]. Nature, 2016, 529(7587): 509-514.

[48] Li S J, He J Z, Zhang M J, et al. Electrochemical detection of dopamine using water-soluble sulfonated graphene[J]. Electrochimica Acta, 2013, 102: 58-65.

有序介孔碳/石墨烯/镍泡沫的制备及其对多巴胺的高灵敏度和高选择性检测

王来玉[1],奚 馨[1],吴东清[2],刘雄宇[1],纪 伟[1],刘瑞丽[1*]

(1. 上海交通大学电子工程系,上海 200240;2. 上海交通大学化学化工学院,上海 200240)

摘要:柔性生物传感器在可穿戴电子设备中有着广泛的应用前景. 为了获得柔性电化学多巴胺传感器,作者在本工作中首先在镍泡沫表面通过化学气相沉积生长石墨烯, 随后通过高温碳化嵌段共聚物与酚醛树脂在石墨烯表面共组装形成的薄膜制备了有序介孔碳/石墨烯/镍泡沫(OMC/G/Ni)复合材料. 其中,镍泡沫可以为复合材料提供具有高导电性和良好柔韧性的金属骨架, 而具有垂直排列介孔阵列的有序介孔碳层为复合材料提供了高的电活性表面积,且有利于活性位点的暴露. 值得注意的是,夹在有序介孔碳层和镍泡沫之间的石墨烯极大地增强了各组分之间的相容性, 有利于进一步提升复合材料的电化学性能. 作为电化学传感器中的工作电极,OMC/G/Ni 体现出优异的多巴胺检测能力. 不但具有宽的线性检测范围(0.05 ~ 58.75 μmol·L^{-1})和低检测限(0.019 μmol·L^{-1}),还具有良好的选择性、重现性和稳定性. 此外,OMC/G/Ni 在弯曲状态下依旧能够保持对多巴胺的高检测能力,证明了其在柔性生物传感器中的应用潜力.

关键词:有序介孔碳;石墨烯;镍泡沫;多巴胺传感器;柔性电化学传感器